Mutational Analysis of Lassa Virus Glycoprotein Highlights Regions Required for Alpha-Dystroglycan Utilization

Marissa Acciani,[a] Jacob T. Alston,[a] Guohui Zhao,[a] Hayley Reynolds,[a] Afroze M. Ali,[a] Brian Xu,[a] Melinda A. Brindley[b]

Department of Infectious Diseases, College of Veterinary Medicine, University of Georgia, Athens, Georgia, USA[a]; Department of Infectious Diseases, Department of Population Health, Center for Vaccines and Immunology, College of Veterinary Medicine, University of Georgia, Athens, Georgia, USA[b]

ABSTRACT Lassa virus (LASV) is an enveloped RNA virus endemic to West Africa and responsible for severe cases of hemorrhagic fever. Virus entry is mediated by the glycoprotein complex consisting of a stable-signal peptide, a receptor-binding subunit, GP1, and a viral-host membrane fusion subunit, GP2. Several cellular receptors can interact with the GP1 subunit and mediate viral entry, including alpha-dystroglycan (αDG) and lysosome-associated membrane protein 1 (LAMP1). In order to define the regions within GP1 that interact with the cellular receptors, we implemented insertional mutagenesis, carbohydrate shielding, and alanine scanning mutagenesis. Eighty GP constructs were engineered and evaluated for GP1-GP2 processing, surface expression, and the ability to mediate cell-to-cell fusion after low-pH exposure. To examine virus-to-cell entry, 49 constructs were incorporated onto vesicular stomatitis virus (VSV) pseudoparticles and transduction efficiencies were monitored in HAP1 and HAP1-ΔDAG1 cells that differentially produce the αDG cell surface receptor. Seven constructs retained efficient transduction in HAP1-ΔDAG1 cells yet poorly transduced HAP1 cells, suggesting that they are involved in αDG utilization. Residues H141, N146, F147, and Y150 cluster at the predicted central core of the trimeric interface and are important for GP-αDG interaction. Additionally, H92A-H93A, 150HA, 172HA, and 230HA displayed reduced transduction in both HAP1 and HAP1-ΔDAG1 cells, despite efficient cell-to-cell fusion activity. These mutations may interfere with interactions with the endosomal receptor LAMP1 or interfere at another stage in entry that is common to both cell lines. Insight gained from these data can aid in the development of more-effective entry inhibitors by blocking receptor interactions.

IMPORTANCE Countries in which Lassa virus is endemic, such as Nigeria, Sierra Leone, Guinea, and Liberia, usually experience a seasonal outbreak of the virus from December to March. Currently, there is neither a preventative vaccine nor a therapeutic available to effectively treat severe Lassa fever. One way to thwart virus infection is to inhibit interaction with cellular receptors. It is known that the GP1 subunit of the Lassa glycoprotein complex plays a critical role in receptor recognition. Our results highlight a region within the Lassa virus GP1 protein that interacts with the cellular receptor alpha-dystroglycan. This information may be used for future development of new Lassa virus antivirals.

Address correspondence to Melinda A. Brindley, mbrindle@uga.edu.

M.A. and J.T.A. contributed equally to this work.

Lassa fever is a hemorrhagic disease caused by an Old World (OW) arenavirus known as Lassa virus (LASV). The virus was first isolated in Nigeria in 1969 and is currently endemic in West Africa (1). Serological studies suggest that hundreds of thousands of

people are infected each year (2). While most infections are mild or asymptomatic, 15 to 20% of cases require hospitalization and result in approximately 5,000 deaths annually (3–5). The rodent host for LASV is the multimammate rat, *Mastomys natalenis* (6). Recently, the virus has been isolated from *Hylomyscus pamfi* and *Mastomys erythroleucus*, potentially increasing its geographic range (7). Human exposure occurs through direct contact with the infected rodents or rodent excrement or close contact with infected patients (8). Due to the high morbidity and mortality associated with Lassa hemorrhagic fever, LASV is classified as a category A pathogen (9).

Lassa virus is an enveloped ambisense RNA virus with a bisegmented genome. Viral particles are covered in mature glycoprotein (GP) trimeric spikes, which mediate viral entry. Like other class 1 viral fusion proteins, the envelope glycoprotein precursor (GPC) is translated as a single polypeptide and is proteolytically cleaved into three subunits. Processing occurs first in the endoplasmic reticulum (ER) by a cellular signal peptidase. GPC is then trafficked to the *cis*-Golgi apparatus and processed by cellular proprotein convertase subtilisin kexin isozyme-1/site-1 protease (SKI-1/S1P) to produce a noncovalent stable-signal peptide (SSP)/GP1/GP2 heterotrimer (Fig. 1A and B) (10–13). Unlike other class I fusion proteins, the relatively long signal peptide of GPC is not degraded; it serves a chaperone-like function necessary for the correct trafficking and processing of GP (14–16). SSP interacts with the cytoplasmic domain of GP2 and is involved in pH sensing (17–19). GP1 is responsible for binding to cellular receptors (20, 21), while GP2 mediates membrane fusion during viral entry (22–24).

Cellular entry of LASV is a multistep process involving multiple GP1-receptor interactions. First, GP1 interacts with a cell surface receptor on the plasma membrane, mainly alpha-dystroglycan (αDG) (21). Additional surface receptors can mediate LASV entry in the absence of αDG, including heparin sulfate, dendritic cell-specific intercellular adhesion molecule-3-grabbing nonintegrin (DC-SIGN), and Tyro3/Axl/Mer (TAM) family members (20, 25, 26). This initial GP1-receptor interaction induces viral internalization through a clathrin-, caveolin-, and dynamin-independent process (20, 27, 28). Once within the low-pH environment of the endolysosomal compartment, GP undergoes conformational changes that reduce its affinity for αDG and increase its affinity to a second receptor, lysosome-associated membrane protein 1 (LAMP1) (29, 30). Engagement of LAMP1 by LASV GP1 is hypothesized to lower the activation energy needed to mediate GP2 conformational changes that fuse the viral and cellular membranes, completing the entry pathway (31).

Previous studies have provided new structural information for both the prefusion conformation and pH-induced changes in the LASV glycoprotein. Recently, the trimeric prefusion GP1/GP2 crystal of LASV was solved (32). This structure provides novel insight into the LASV GP complex, including trimer organization, glycosylation, and potential receptor binding sites. The LASV GP1 monomeric protein was previously crystallized under low-pH conditions (pH 5) (33). The low-pH-purified protein was unable to interact with αDG but interacted with LAMP1, suggesting that the crystal structure resembles GP1 in the lysosome (33). Comparison of the prefusion GP1 crystal (isolated at pH 8) and the pH 5 GP1 crystal structure highlights several low-pH-induced conformational changes required for LAMP1 interactions (32).

In addition to the crystallization studies, a cryo-electron tomography (cryo-ET) study was able to construct three-dimensional structures of LASV GP trimers under increasingly acidic pH conditions (pH 7, 5, and 3) (31). Tomographic reconstructions suggest that the GP1 subunit undergoes conformational changes at pH 5, opening a putative LAMP1 binding crevice at the GP1 trimeric interface (31, 33). Pseudoatomic models fit both prefusion GP1/GP2 and low-pH GP1 crystal structures into the low-resolution cryo-ET densities, providing three-dimensional models of GP trimer organization (22, 31–33).

LASV entry is most efficient when GP1 interacts with αDG and LAMP1. While the GP1 binding interface has been mapped in both αDG and LAMP1, the corresponding receptor-binding sites in GP1 have yet to be elucidated. Utilizing the new crystal structure as a model, we used carbohydrate shielding, insertional mutagenesis, and
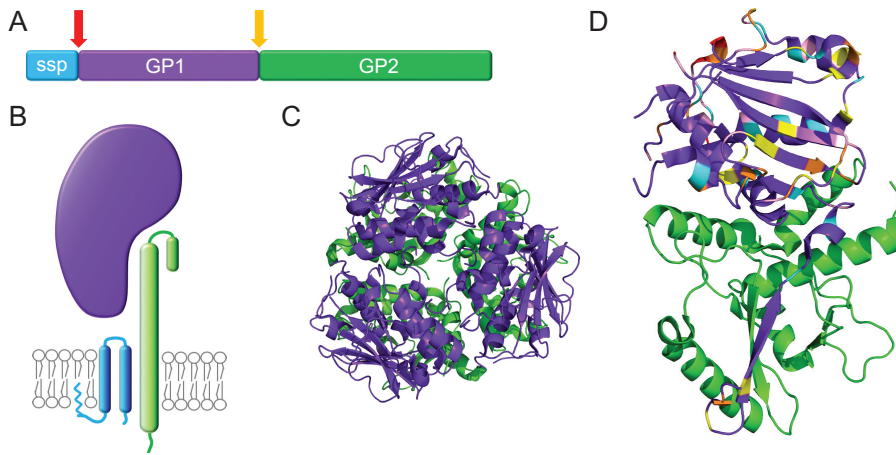
FIG 1 Subunits and structure of the Lassa virus glycoprotein complex. (A) The LASV glycoprotein complex consists of the membrane-integrated stable-signal peptide (SSP) (blue), the GP1 subunit (purple), and the noncovalently attached GP2 subunit (green). The GPC is cleaved by the signal peptidase (red arrow) and SKI-1/S1P (yellow arrow) during protein processing. (B) Cartoon of the SSP, GP1, and GP2 heterotrimer complex in the lipid bilayer. (C) Trimeric LASV GP1-GP2 crystal structure, viewed from the top down; GP1 is in purple and GP2 in green (PDB 5vk2) (32). (D) LASV GP1-GP2 crystal structure, side view (PDB 5vk2). The engineered GP1 constructs are color coded as follows: pink, glycosylation site removals and additions; orange, HA-tagged sites; yellow, alanine scanning of charged residues; blue, alanine scanning of hydrophobic residues; red, additional targeted residues. Note that many of the targeted residues were found in regions of the structure that did not crystallize. All structures were rendered with PyMol.

alanine scanning mutagenesis to identify regions within GP1 important for receptor interactions (Fig. 1D).

RESULTS

With the overarching goal of understanding the functional and spatial organization of the arenavirus prefusion glycoprotein structure, we utilized the trimeric GP prefusion crystal structure (32) to identify residues involved in receptor interactions.

Function of GPC N-linked glycans. Arenavirus GP N-linked glycans play significant biochemical roles in virus-cell interactions (34, 35). Previous studies found that specific N-linked glycans in LCMV GP1 were necessary for GP trafficking, fusion activity, and infectivity (34). LASV GP1 contains seven conserved N-linked glycosylation sites. Removing glycans at positions 81, 91, 101, and 121 was previously shown to inhibit GPC processing into GP1 and GP2 (35), although receptor binding and fusion activity were not evaluated. We reproduced the seven N-glycan mutants by changing glycosylation site motifs from N-X-S/T to N-X-A. To examine the level of processed GP on the cell surface, surface proteins were biotinylated, concentrated using streptavidin Sepharose beads, and subjected to immunoblot analysis (Fig. 2A). All mutated GPs migrated faster than parental GP, confirming that all seven sites are glycosylated. We similarly found that removing the N-linked sites at T81 and S91 resulted in GPC processing defects (Fig. 2A and C). However, we found that the remaining five N-glycan mutations resulted in detectable levels of GP1-GP2 processing, including T101 and S121. Our use of a codon-optimized expression construct and examining surface material 36 h after transfection, rather than 24 h, may have enabled T101A and S121A mutants to reach detectable steady-state levels of processed GP1-GP2 at the cell surface (35).

To determine if the constructs lacking N-glycans produce functional GP, we determined if they could produce syncytia, or multinucleated cells, in a cell-to-cell-based fusion assay. Incubating LASV GP-transfected cells with a low-pH buffer results in efficient GP activation and robust syncytium formation (Fig. 2B). By comparing the extent of syncytium formation between mutant and parental GPs, we can determine the fusion efficiency of each mutant. The fusion activity of the N-glycan mutants closely correlated with the cleavage efficiency (Fig. 2C), suggesting that the glycans are not required for productive cell-to-cell fusion.
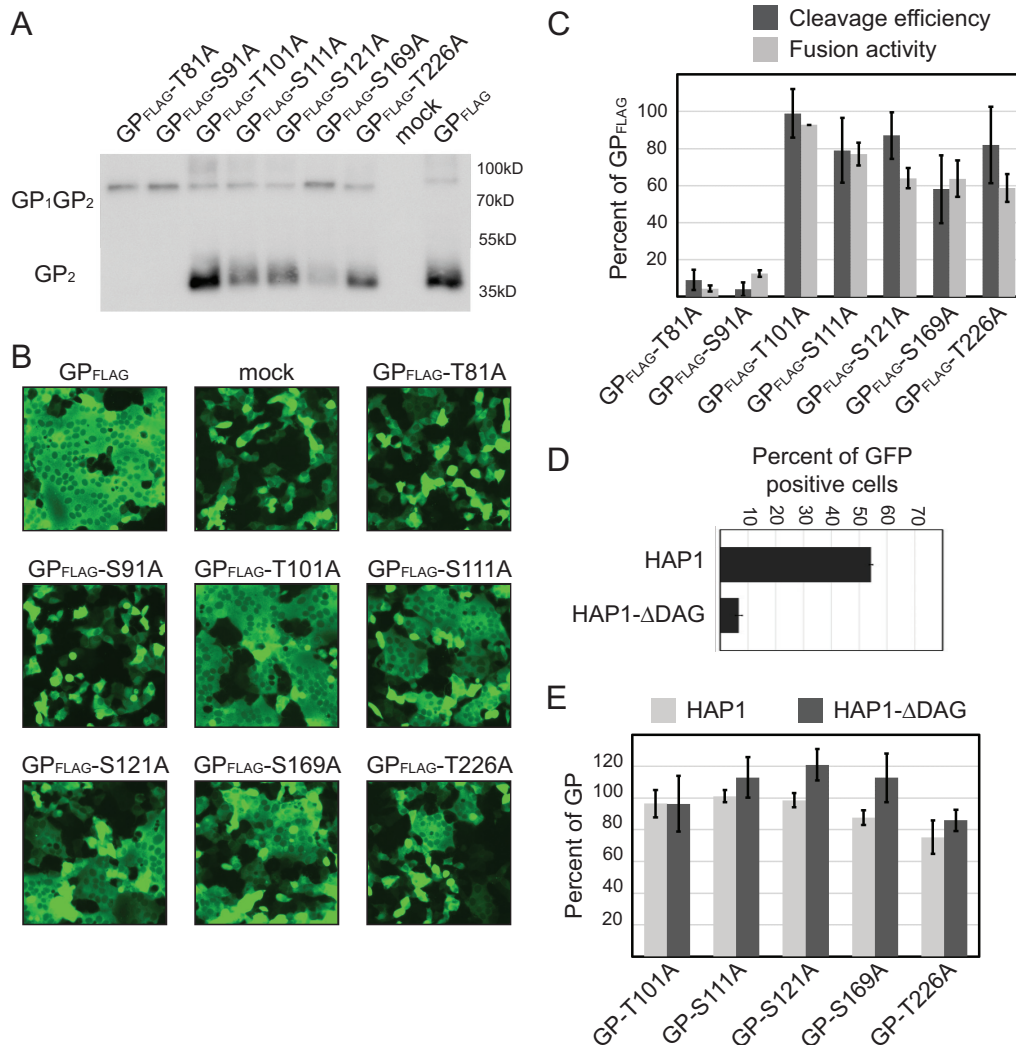
FIG 2 Processing and functional characteristics of surface-expressed GP1 N-glycosylation sites. (A) Vero cells were transfected with the indicated FLAG-tagged LASV GP variant or the negative control. After 36 h, cells were subjected to surface biotinylation. Surface-expressed biotinylated proteins were concentrated using streptavidin Sepharose beads. Precipitated proteins were separated by SDS-PAGE. Immunoblot assays were carried out to detect LASV GP surface-expressed protein using an anti-FLAG antibody, M2. The immunoblot shown is representative of four trials. (B) Microphotographs of Vero cells cotransfected with plasmid DNA encoding LASV GP construct and GFP. Cell-to-cell fusion was assessed 3 h following low-pH-medium shock; magnification, ×20. Representative fields of view are shown. (C) Fusion data for each construct was quantified by counting unfused cells and comparing the numbers to those in mock-transfected wells. Quantified fusion data for each construct were normalized to LASV wt-GPC-3xFLAG. Cleavage efficiency was normalized to FLAG-tagged GP using densitometry analysis. (D) Parental GP transduction efficiency in HAP1 and HAP1-ΔDAG1 cells. VSVΔG-GFP pseudoparticles containing LASV GP were added to both cells, and the GFP-positive cells were enumerated in a flow cytometer. The percentage of the cell population that was GFP positive is shown. (E) VSVΔG-GFP pseudoparticles containing LASV GP or N-glycosylation mutants were used to transduce HAP1 and HAP1-ΔDAG1 cells. The GFP-positive cells were enumerated in a flow cytometer. Transduction efficiencies were normalized to parental LASV GP particle transduction values in each respective cell type. All data are based on the averages and standard errors of the means from at least three replicate experiments.

Cell-to-cell fusion assays do not completely recapitulate the process that occurs when a viral particle fuses with an endosomal membrane. Virus-to-cell entry requires the viral glycoprotein to facilitate interactions with cellular receptors to initiate endocytosis. Once trafficking to the proper cellular compartment occurs, LASV must undergo a receptor switch in the endolysosome before membrane fusion. In order to determine if the GP1 constructs can mediate viral entry, vesicular stomatitis virus (VSV) pseudotyped particles were produced containing LASV GP on their surface. Particle transduction was monitored in two haploid cell lines, HAP1 and HAP1-ΔDAG1. LASV entry into HAP1 cells and HAP1-ΔDAG1, a cell line deficient in αDG, has been thoroughly

documented by recent genetic screens (20, 36). Gene trap screening of HAP1 cells reconfirmed that LASV GP's interaction with properly glycosylated αDG significantly enhances cell entry (36). A second genetrap screen in HAP1-ΔDAG1 cells identified an additional, lysosomal receptor, LAMP1 (20). Because efficient HAP1 entry of LASV occurs through αDG interactions and HAP1-ΔDAG1 cell entry occurs through other cell surface receptors, such as heparin sulfate receptors (20), we propose that constructs exclusively demonstrating reduced transduction efficiency into HAP1 cells are inefficiently engaging αDG. In order to demonstrate the entry enhancement by αDG, we added the same volume of pseudotyped particles coated with LASV GP on both cell lines (Fig. 2D). LASV GP entry into HAP1 cells produced 8.4 $\pm$ 0.83 times more green fluorescent protein (GFP)-positive cells than the same volume of particles added to HAP1-ΔDAG1 cells. To compensate for the decreased entry into HAP1-ΔDAG1 cells, we increased the volume of particles used to transduce this cell type. When examining the transduction efficiencies, each mutant GP was compared to parental GP in each cell type, so that specific defects in HAP1 cell entry would highlight mutations that facilitated viral uptake through αDG interactions.

Because GP can only fuse if GP1-GP2 processing occurs, we examined transduction efficiency for constructs with at least 50% cleavage efficiency. Five glycosylation removal GP1 constructs were examined in transduction assays, T101A, S111A, S121A, S169A, and T226A mutants. All five constructs efficiently transduced both cell types, suggesting that GP missing a single N-glycan retains cell entry (Fig. 2E).

Engineering N-linked glycosylation sites onto GP1. Carbohydrate shielding, or glycosylation site additions, can be used to map glycoprotein structural domains (37–39). We engineered seven additional glycosylation sites throughout GP1 (Fig. 3). All glycosylation sites were predicted to be present on the surface of the GP1 model, although H141N, N148S, V187T, and Y253N had potential to impede trimer formation based on the new trimeric structure (32). The mutants were evaluated for the incorporation of the glycan, as well as processing with surface biotinylation assays (Fig. 3A). Glycosylation additions were confirmed by the slow mobility pattern of GP1-GP2 on an immunoblot compared to that of parental GP, which was observed for H141N, V187T, D211S, and Q232N mutants (Fig. 3A). The remaining constructs, K116S, N148S, and Y253N mutants, were not glycosylated, suggesting that these motifs were not recognized by cellular glycotransferases. The trimeric structure predicts N148 and Y253 to be located at the center of the trimer, possibly making these residues inaccessible. K116 was also not glycosylated, despite its predicted location on top of the trimer with clear access to glycotransferases. The natural glycosylation site at N119 may sterically prevent neighboring glycan additions.

Cleavage was reduced for all glycosylated constructs except for the D211S mutant, indicating that the additional glycans reduced SKI-1/S1P recognition or efficient GP trafficking to the Golgi apparatus in most cases. Cell-to-cell fusion activity was proportional to cleavage efficiency, suggesting that the additional glycans did not prevent GP2 activation at low pH if GP1-GP2 processing occurred (Fig. 3B). Although Y253N did not appear to be glycosylated, the mutation decreased fusion relative to the amount of cleaved GP, suggesting that the point mutation alone may decrease the efficiency of GP refolding and completing the fusion process.

Transduction assays were performed with K116S, N148S, D211S, and Y253N mutants, which demonstrated >50% GP processing (Fig. 3C). Both D211S and Y253N mutants reduced transduction compared to parental GP, yet transduction levels between HAP1 and HAP1-ΔDAG1 cells were similar. This suggests that mutations were not altering interactions with αDG but inhibiting an entry step common in both cell types. The Y253 construct's reduced fusion activity may account for reduced transduction levels, while the additional glycan on D211S may have decreased transduction efficiency in both cell lines.

Characterization of GP1 using insertional mutagenesis. Few of the additional N-linked glycosylation sites that we engineered were efficiently glycosylated (Fig. 3).
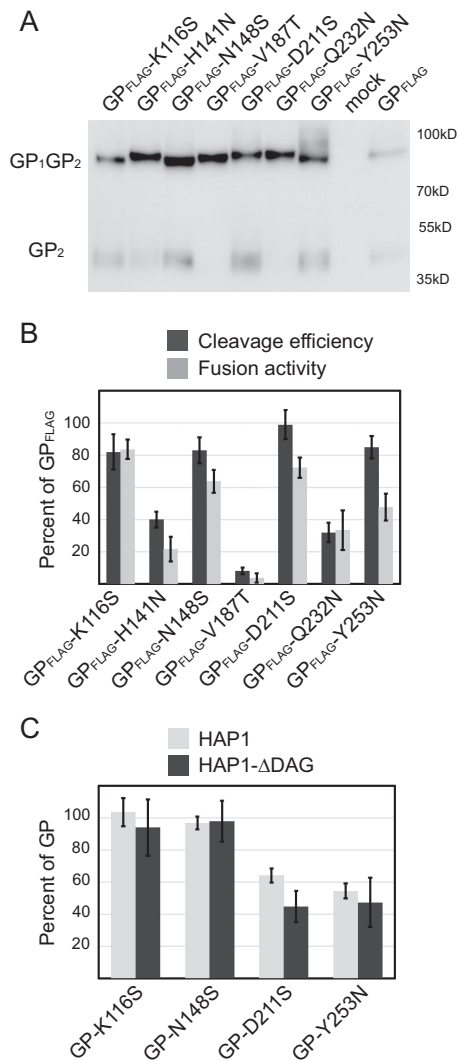
FIG 3 Functional analysis of GP1 containing engineered N-linked glycosylation sites. (A) Surface-expressed GP of N-glycan mutants and immunoblot analysis using anti-FLAG antibody M2 for detection. (B) Cleavage efficiency and cell-to-cell fusion data. (C) Transduction of HAP1 and HAP1-ΔDAG1 cells using VSV-pseudotyped particles. All data are based on the averages and standard errors of the means from at least three replicate experiments.

Therefore, we employed insertional mutagenesis to add bulky epitope tags throughout GP1 to impede receptor binding (Fig. 4). The nine-amino-acid hemagglutinin (HA) epitope tag (YPYDVPDYA) was inserted at 21 positions along the length of GP1. Insertion sites were chosen to avoid perturbation or disruption of protein tertiary structures. To increase the flexibility of the HA tag, 14 insertions included Gly-Gly-Ser linkers (IHA) flanking the insertion.

Surface expression of HA insertion constructs varied. Most constructs were produced, but the majority of insertions resulted in processing defects, evidenced by the lack of cleaved GP2 in surface biotinylated material (Fig. 4A). Although the HA insertion sites were added to unstructured surface loops, the insertions appeared to alter protein folding in the majority of the constructs, preventing GPC processing by SKI-1/S1P. Overall, only 7 of the 21 mutants displayed appreciable cleavage compared to parental GP (Fig. 4A).

To test for GP fusion activity, the mutant constructs were expressed in Vero cells and incubated with a low-pH buffer to trigger conformational changes. As expected, mutations that inhibited GPC cleavage did not display any fusion activity (Fig. 4B).
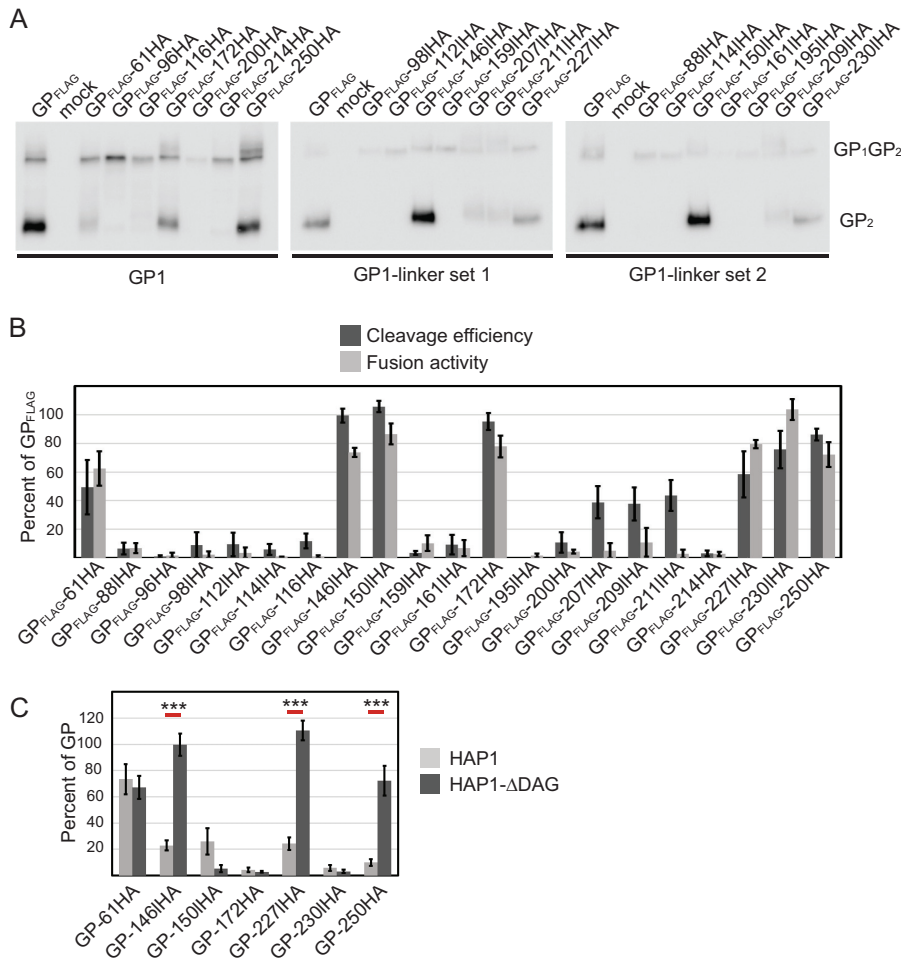
FIG 4 Insertional mutagenesis of LASV GPC blocks entry in specific cell lines. (A) Surface-expressed HA-tagged mutants and immunoblot analysis using anti-FLAG antibody M2. (B) Cleavage efficiency and cell-to-cell fusion data. (C) Transduction of HAP1 and HAP1-ΔDAG1 cells using VSV-pseudotyped particles. All data are based on the averages and standard errors of the means from at least three replicate experiments. ***, $P < 0.001$.

Constructs that retained GPC processing all produced syncytia, suggesting that the HA insertions did not prevent the low-pH conformational changes when SKI-1/S1P recognition occurred (Fig. 4B).

Transductions were carried out for 7 of the 21 insertion constructs. Only one construct, 61HA, was able to transduce both cell lines (Fig. 4C). The GP1/GP2 crystal structure indicates that the N-terminal region of GP1 produces an extended β-sheet that interacts with GP2 (32) (Fig. 1D). Therefore, the HA epitope tag addition after residue 61 would be near the viral membrane and separated from the main body of GP1. Three constructs, 146HA, 227HA, and 250HA, were able to transduce HAP1-ΔDAG1 cells but were unable to efficiently transduce HAP1 cells, suggesting that these insertions inhibit αDG utilization (Fig. 4C). As expected, HAP1 transduction was not completely eliminated. Lassa virus entry into HAP1 can occur through an alternative pathway that does not require αDG (20, 36). Therefore, particles that have reduced affinity for αDG may still be able to enter HAP1 cells through the alternative, albeit less efficient pathway. The remaining three constructs, 150HA, 172HA, and 230HA, showed low to no transduction in both HAP1 cell lines, suggesting that the inserts inhibited a step in the entry process that is common to both cell lines, such as LAMP1 interaction (Fig. 4C).

Alanine scanning of hydrophobic and charged residues. Large insertions and glycan additions tended to block GP cleavage, preventing full GP characterization. To
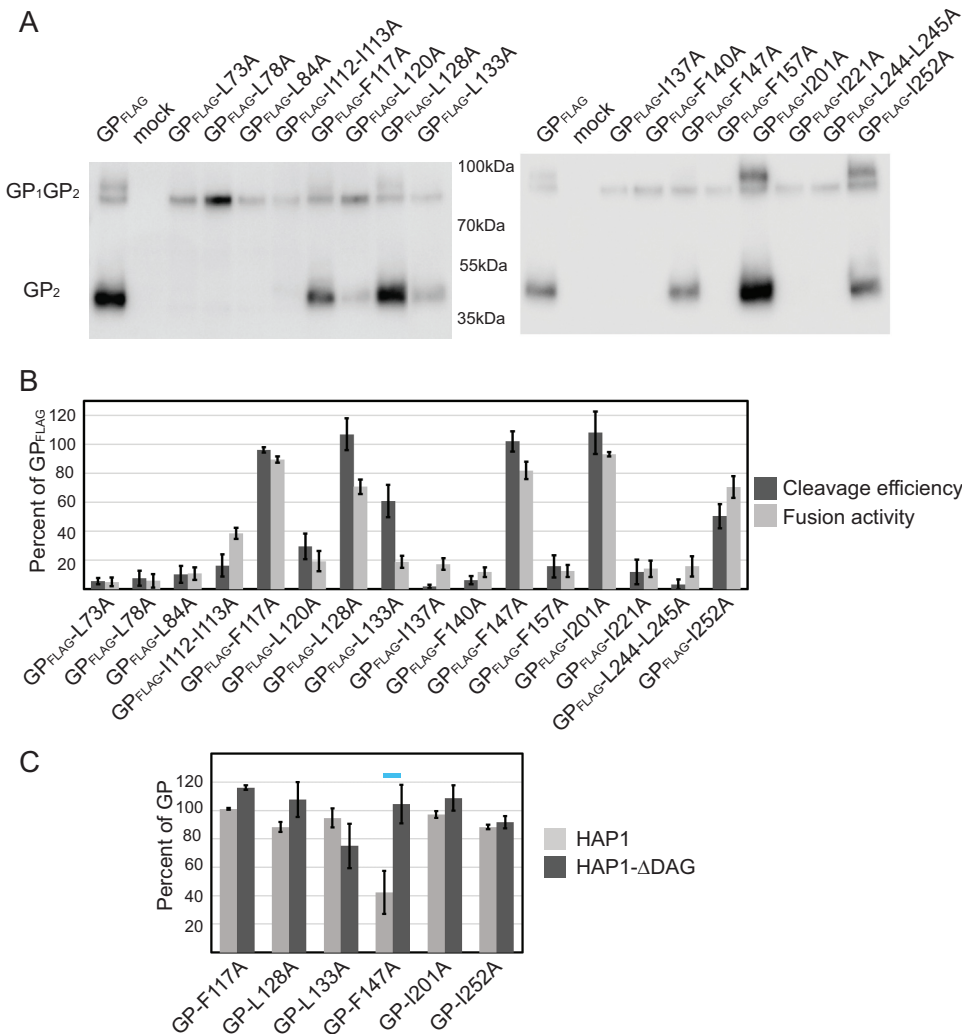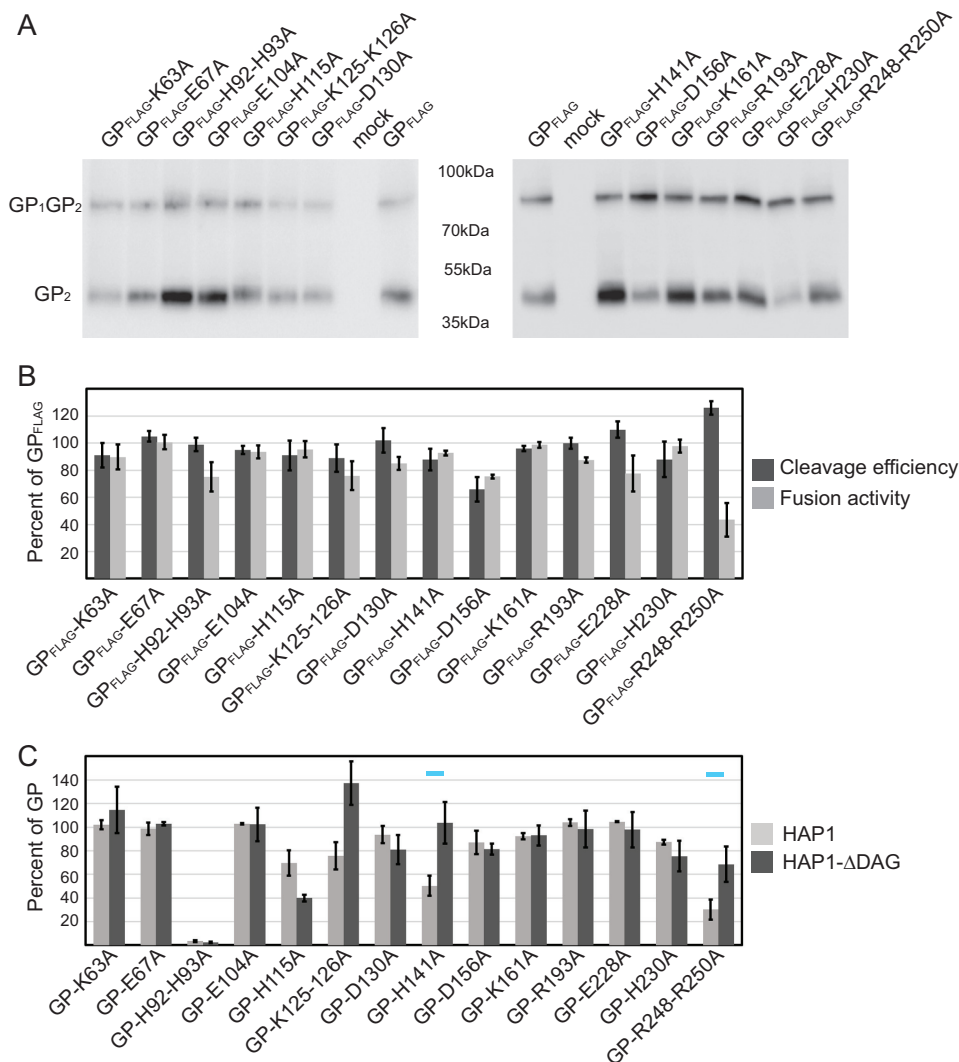
FIG 5 Mutating hydrophobic GP1 residues impedes protein processing. (A) Surface-expressed hydrophobic mutants and immunoblot analysis using anti-FLAG antibody M2. (B) Cleavage efficiency and cell-to-cell fusion data. (C) Transduction of HAP1 and HAP1-ΔDAG1 cells using VSV-pseudotyped particles. All data are based on the averages and standard errors of the means from at least three replicate experiments. The horizontal blue bar highlights the construct that transduced HAP1-ΔDAG1 in a fashion similar to that of parental GP yet showed a defect in HAP1 entry.

increase the chances of producing GP trimers that are trafficked to the cell surface in a processed state, we introduced single-amino-acid substitutions. Hydrophobic and charged residues can be critical for virus glycoprotein-receptor interactions and entry (40–44). To locate possible αDG binding sites in LASV GP1, alanine scanning was used to mutate conserved hydrophobic and charged residues. Of 16 hydrophobic mutants, 11 demonstrated a >50% reduction in cleavage efficiency and/or fusion activity compared to that of parental GP (Fig. 5A and B). Several of the hydrophobic residues were located in secondary structures of GP1, and presumably alanine substitutions resulted in protein misfolding. For the remaining mutants, those that produced cleaved GP2 were able to form syncytia. The L133A mutant produced little protein and, along with the decreased cleavage efficiency (60% of parental GP), resulted in very low fusion activity.

Six hydrophobic mutants were examined in transduction assays. The majority of the hydrophobic mutations transduced both cell lines as well as wild-type GP (Fig. 5C). The low protein level seen with L133A did not significantly impact transduction efficiency. While the F147A mutant was able to transduce HAP1-ΔDAG1 cells at a level similar to
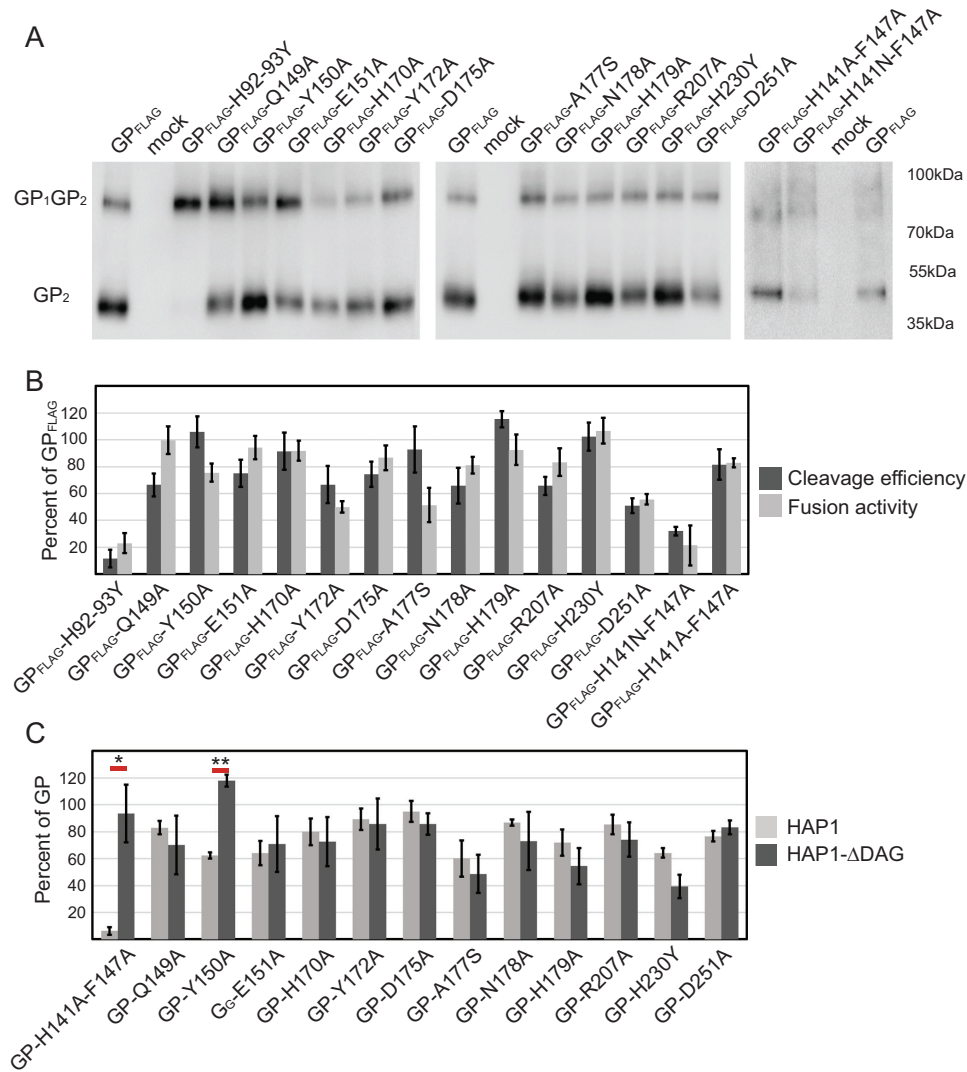
FIG 6 Charged GP1 residues are required for efficient HAP1 entry. (A) Surface-expressed charged mutants and immunoblot analysis using anti-FLAG antibody M2. (B) Cleavage efficiency and fusion ability data. (C) Transduction of HAP1 and HAP1-ΔDAG1 cells using VSV-pseudotyped particles. All data are based on the averages and standard errors of the means from at least three replicate experiments. The horizontal blue bars highlight the constructs that transduced HAP1-ΔDAG1 more than twice as efficiently as HAP1 cells.

that of wild-type GP, transduction in HAP1 cells was reduced to 42%. The transduction defect in HAP1 cells with no defect in HAP1 ΔDAG1 cells suggests that F147 is important for efficient αDG utilization.

Fourteen conserved charged residues were mutated to alanine, including a described histidine triad (H92, H93, and H230), which has been implicated in LAMP1 interaction (30, 33). All mutated GPs were cleaved and transported to the cell membrane at levels greater than 60% of parental GP (Fig. 6A). The charged residue mutants also displayed high levels of cell-to-cell fusion activity (Fig. 6B). Only the GP R248A-R250A mutant demonstrated reduced fusion.

We produced VSV pseudoparticles expressing all 14 charged mutations and tested their ability to transduce HAP1 and HAP1-ΔDAG1 cells (Fig. 6C). The H92A-H93A mutant was unable to transduce either cell type tested. The H230A (third residue of the described histidine triad) mutant showed relatively high levels of transduction. K125A-K126A, H141A, and R248A-R250A mutants demonstrated a reduced transduction in HAP1 cells compared to HAP1-ΔDAG1 cells. Although transduction into HAP1 cells was not completely inhibited, the data suggest that the mutations may decrease efficient interaction with αDG.

FIG 7 Residues involved with the GP1 trimer core are critical for αDG interaction. (A) Surface-expressed targeted GP1 mutants and immunoblot analysis using anti-FLAG antibody M2. (B) Cleavage efficiency and fusion ability data. (C) Transduction of HAP1 and HAP1-ΔDAG1 cells using VSV-pseudotyped particles. All data are based on the averages and standard errors of the means from at least three replicate experiments. *, $P < 0.05$; **, $P < 0.01$.

Additional targeted mutations. The transduction data suggested that residues located near the center of the GP1 trimer were key for efficient αDG entry. To more fully examine this region, an additional 15 point mutations that focused on the regions surrounding the top of the GP1 trimer and residues adjacent to mutations that reduced transduction in HAP1 cells were created (Fig. 7). To determine if combining some of the individual mutations that modestly decreased HAP1 entry would synergistically eliminate αDG binding, two double mutants that incorporated mutations at GP residues 141 and 147 were made. Constructs with H92Y-H93Y and H230Y mutations were also made to compare the effects of alanine versus tyrosine substitutions and to reproduce similar constructs tested in the study by Cohen-Dvashi et al. (30, 33). Overall, surface expression and processing of the additional targeted mutants were near wild-type LASV GP levels with the exception of H92Y-H93Y and H141N-F147A mutants. Both of these double mutants were produced but were poorly processed (Fig. 7A). When the asparagine at position H141 in the double mutant was changed to alanine, surface expression, processing, and fusion increased. Histidines at positions 92 and 93, when changed to alanines, retained processing and fusion activity (Fig. 6B), but tyrosine substitution led to GPC processing defects (Fig. 7A). Previous work by Cohen-Dvashi et al. tested
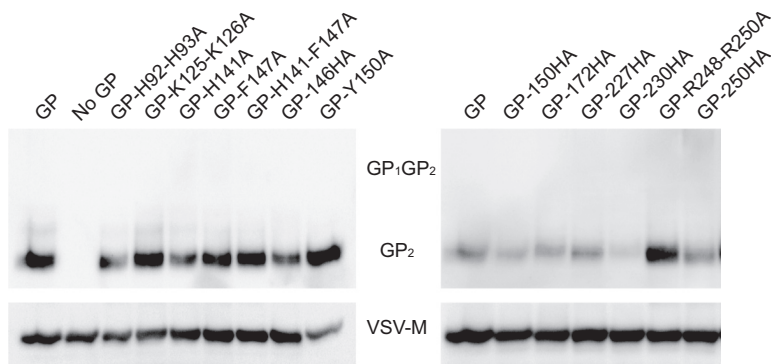
FIG 8 GP constructs are efficiently incorporated onto VSV particles. Vero cells were used to produce VSV pseudoparticles. Cell supernatants, containing pseudotyped particles, were collected and precipitated with TCA to determine the level of LASV GP incorporation into VSV envelopes. GP constructs demonstrating low HAP1 transduction or GP constructs that were unable to transduce both cell types were tested. Precipitated proteins were separated by SDS-PAGE and immunoblotted for LASV GP2 (monoclonal antibody 12.4D) and VSV-M (monoclonal antibody 23H12).

individual mutations H92Y, H93Y, and H230Y for processing, surface expression, and fusion activity (30). When they individually changed each histidine to tyrosine, they found a reduction in the level of cleaved, surface-expressed GP but no significant changes in cell-cell fusion. Our H92Y-H93Y double mutant completely inhibited GP processing as well as fusion (Fig. 7A and B). Similar to what was seen in the previous study, H230Y was efficiently processed and induced cell-to-cell fusion at levels greater than wild-type GP. In general, fusion activity, with the exception of that seen with A177S, again closely correlated with cleavage efficiency (Fig. 7B).

Of the 15 constructs made, 13 were tested in transduction assays. Only two constructs, Y150A and H141A/F147A mutants, showed reduced transduction in HAP1 cells compared to HAP1-ΔDAG1 cells (Fig. 7C). The combination of H141A and F147A had an additive effect. Individual changes dropped HAP1 transduction to 40% of parental GP, and the double mutant dropped HAP1 transduction to 10% of parental GP while retaining near-wild-type levels of HAP1-ΔDAG1 transduction. All other constructs were able to transduce HAP1 and HAP1-ΔDAG1 cells with similar efficiencies (Fig. 7C). While H230Y did not result in cell type-specific transduction defects, this mutation moderately reduced transduction in both cell lines, similar to the observations in the previous study (30).

GP incorporation onto VSV particles. While many of the constructs produced particles that transduced both cell types, some constructs did not efficiently transduce either cell line, or they displayed a deficiency in a specific cell type. To ensure that the low-transducing constructs incorporated sufficient levels GP on the particle, immunoblot assays were performed (Fig. 8). All particles incorporated the mutated GP constructs, including those constructs that failed to transduce both cell lines. Constructs with K125A-K126A and Y150A mutations, two mutants that demonstrated a reduction in HAP1 transduction and an enhancement in HAP1-ΔDAG1 cells, were consistently found on VSV particles at higher levels than wild-type GP. Similarly, the R248-R250A mutant was found on particles at a higher rate that parental GP, although it did not transduce better than the wild type.

Residues H141-F147 and R248-R250 are critical for αDG interaction. In order to directly assess the ability of GP mutants to bind with αDG, we performed a coimmunoprecipitation experiment. Beads coated with αDG were incubated with VSV-pseudotyped particles containing either parental or mutant GP. We examined GP-H141A-F147A and GP-R248A-R250A, because they each contained point mutations that resulted in HAP1 entry defects. In addition, we evaluated GP-H230Y, a construct implicated in LAMP1 binding. Parental GP and GP-H230Y were efficiently precipitated by αDG, whereas we were unable to biochemically detect GP-H141A-F147A and
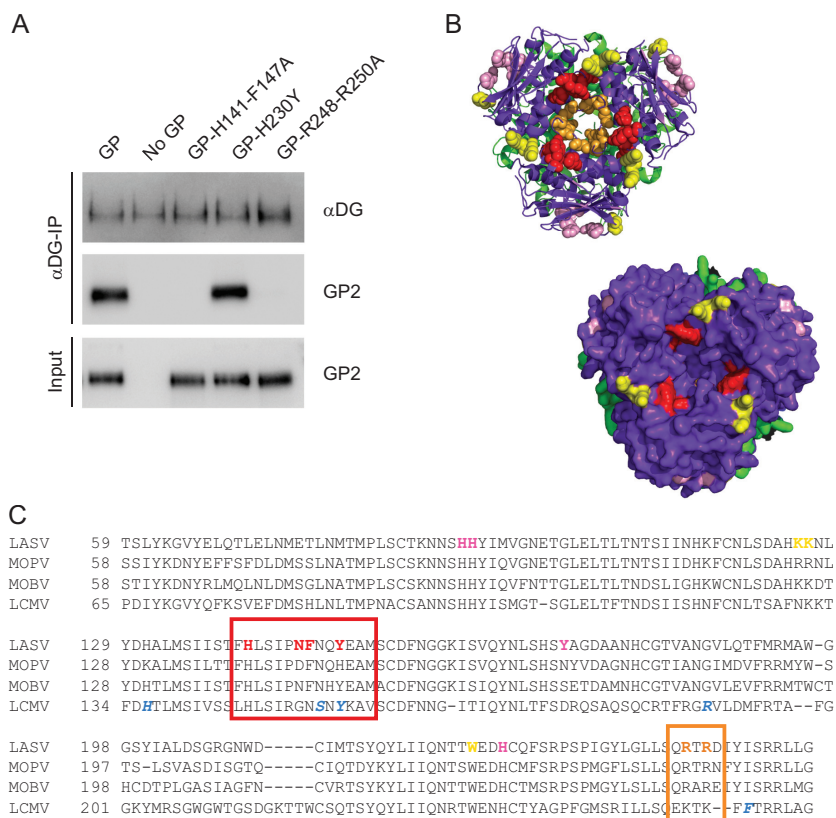
FIG 9 Identification and mapping residues implicated in LASV receptor binding and viral entry. (A) To directly examine GP1 mutant binding, or lack of binding, to αDG, we performed a coimmunoprecipitation assay. αDG-coated beads were incubated with VSV-pseudotyped particles containing either parental or mutant LASV GP. All proteins interacting with the αDG-coated beads were concentrated and separated by SDS-PAGE. While parental GP and GP-H230Y were able to bind to αDG, GP-H141A-F147A and GP-R248A-R250A were not. (B) LASV GP constructs exhibiting reduced entry into HAP1 cells were mapped onto the LASV prefusion crystal structure (PDB 5vk2; GP1 is shown in purple, and GP2 is shown in green). Regions that are significantly involved in αDG interactions are shown in red (H141, N146, F147, and Y150). Regions that also demonstrated reduced HAP1 entry are shown in orange (R248 and R250) and yellow (K125, K126, and W227). The histidine triad is shown in pink (H92, H93, and H230). Residues are color coded to match Table 1. Both a cartoon structure and surface rendering of the structure demonstrate that the αDG binding site is located in a cavity on the top of the trimer. (C) Sequence alignment of Old World arenaviruses that use αDG. Regions in LCMV involved in αDG binding are shown in blue, while the regions that we have implicated for LASV entry are shown in red. R248 and R250 are highlighted in orange. The histidine triad implicated in LAMP1 interaction is in pink.

GP-R248A-R250A (Fig. 9A). These data further support our conclusions that the central core of GP mediates interaction with αDG (Fig. 9B).

DISCUSSION

Here we provide data highlighting LASV GP1 residues important for receptor interactions. We produced and characterized a library of 80 constructs. Transduction was monitored in cell lines that differentially express the LASV receptor αDG. Biochemical characterization grouped GP1 mutants into various categories based on their transduction phenotypes (Table 1). The data implicate regions of GP1 that facilitate entry through αDG, as well as residues involved with LAMP1 interaction.

We tested all of the constructs in cell-to-cell fusion assays, and those that were efficiently processed were tested in pseudotype particle entry assays. A number of mutants, including H92A-H93A, 150lHA, 172HA, and 230lHA mutants, produced large syncytia in cell-to-cell fusion assays, yet were unable to facilitate entry when incorporated onto VSV particles. This suggests that the requirements for cell-to-cell fusion and virus-to-cell fusion are different. The luminal pH of most lysosomes ranges from 4.5 to 5 (45). In contrast, we utilized phosphate-buffered saline (PBS) at pH 4 in the cell-to-cell

TABLE 1 Summary of fusion, GP cleavage, and transductions[a]

Mutant	Classification	Fusion Activity	Cleavage Efficiency	Transduction Efficiency		Class
				HAP1	HAP1-ΔDAG	
L61HA	HA insertion	62.4 ± 12.1	49.4 ± 19	73.6 ± 11.5	67.9 ± 8.6	III
K63A	Charged	89.8 ± 9.1	91.3 ± 9.3	102.1 ± 3.8	114.5 ± 19.7	III
E67A	Charged	100.8 ± 5.4	104.9 ± 3.8	98.7 ± 5.2	102.9 ± 1.4	III
H92A-H93A	Charged	75.0 ± 10.9	99.1 ± 5.0	3.4 ± 0.8	2.3 ± 0.6	I
T101A	N-gly removal	92.8 ± 0.1	98.9 ± 13.2	96.5 ± 8.7	96.3 ± 17.6	III
E104A	Charged	93.7 ± 4.8	95.5 ± 3.4	102.8 ± 0.5	102.4 ± 14.2	III
S111A	N-gly removal	77.1 ± 6.1	79.4 ± 17.5	101.2 ± 3.9	112.9 ± 12.8	III
H115A	Charged	95.5 ± 5.9	91.3 ± 10.7	69.6 ± 10.9	39.9 ± 2.7	III
K116S	N-gly addition	83.6 ± 6.0	82.1 ± 11.5	103.5 ± 6.6	93.9 ± 8.8	III
F117A	Hydrophobic	89.4 ± 2.2	96.3 ± 1.8	101.1 ± 0.6	116.1 ± 1.7	III
S121A	N-gly removal	64.0 ± 5.5	86.8 ± 12.5	98.6 ± 4.4	121.0 ± 9.8	III
K125A-K126A	Charged	76.0 ± 10.6	89.5 ± 10.2	75.6 ± 11.4	137.2 ± 18.4	II
L128A	Hydrophobic	70.8 ± 5.0	107.0 ± 11.1	88.3 ± 3.5	107.8 ± 12.4	III
D130A	Charged	85.0 ± 4.8	102.3 ± 9.0	93.7 ± 7.3	81.0 ± 12.4	III
L133A	Hydrophobic	19.0 ± 4.2	61.0 ± 11.2	94.7 ± 6.7	75.0 ± 15.6	III
H141A	Charged	92.7 ± 1.7	87.8 ± 8.3	50.3 ± 8.7	103.7 ± 17.5	II
F147A	Hydrophobic	82.0 ± 5.9	102.1 ± 7.0	42.2 ± 15.1	104.5 ± 13.7	II
H141A-F147A	Targeted	82.8 ± 3.3	81.6 ± 11.4	17.4 ± 2.8	93.5 ± 21.5	II
N146IHA	HA + linker	73.7 ± 3.1	99.4 ± 4.8	23.0 ± 3.8	100.5 ± 11.7	II
N148S	N-gly addition	63.8 ± 7.1	83.3 ± 7.9	96.7 ± 4.9	97.9 ± 11.0	III
Q149A	Targeted	99.6 ± 10.2	66.5 ± 8.5	83.1 ± 4.9	70.1 ± 21.8	III
Y150A	Targeted	75.5 ± 6.7	105.9 ± 11.6	62.2 ± 2.3	117.9 ± 4.4	II
Y150IHA	HA + linker	86.6 ± 7.2	105.8 ± 3.9	26.0 ± 10.1	5 ± 0.8	I
E151A	Targeted	94.1 ± 8.7	75.1 ± 10.1	64.1 ± 9.0	70.9 ± 20.8	III
D156A	Charged	75.4 ± 1.4	66.1 ± 8.5	87.0 ± 9.8	81.4 ± 4.6	III
K161A	Charged	98.6 ± 2.1	96.1 ± 1.8	92.2 ± 2.6	93.0 ± 8.6	III
S169A	N-gly removal	63.7 ± 9.9	58.4 ± 18.4	87.6 ± 4.7	112.8 ± 15.3	III
H170A	Targeted	91.2 ± 7.5	91.5 ± 13.8	80.0 ± 10.0	72.7 ± 18.2	III
Y172A	Targeted	50.0 ± 4.3	66.6 ± 13.8	89.3 ± 7.9	85.5 ± 19.0	III
Y172HA	HA insertion	77.9 ± 7.6	95.4 ± 5.9	4.3 ± 1.8	4.6 ± 2.5	I
D175A	Targeted	86.6 ± 9.1	74.4 ± 9.5	95.1 ± 7.9	85.6 ± 8.0	III
A177S	Targeted	51.4 ± 12.8	92.7 ± 17.2	60.1 ± 13.4	48.6 ± 14.3	III
N178A	Targeted	81.1 ± 6.1	65.9 ± 13.3	86.9 ± 2.4	73.2 ± 21.8	III
H179A	Targeted	92.6 ± 11.4	115.3 ± 6.1	71.9 ± 9.8	54.5 ± 13.3	III
R193A	Charged	87.5 ± 1.9	99.7 ± 3.7	103.9 ± 2.9	98.5 ± 15.6	III
I201A	Hydrophobic	93.3 ± 1.6	108.0 ± 14.8	97.1 ± 2.3	108.8 ± 8.9	III
R207A	Targeted	83.4 ± 10.2	65.8 ± 6.7	85.4 ± 7.2	74.2 ± 12.9	III
D211S	N-gly addition	72.3 ± 6.3	99.5 ± 8.9	64.1 ± 18.5	44.7 ± 9.7	III
T226A	N-gly removal	58.6 ± 7.5	82.4 ± 20.7	75.3 ± 10.6	85.9 ± 6.6	III
W227IHA	HA + linker	79.5 ± 2.9	58.5 ± 16	24.3 ± 4.8	103.7 ± 4.1	II
E228A	Charged	77.7 ± 13.4	109.7 ± 5.8	104.6 ± 0.3	97.8 ± 15.0	III
H230A	Charged	97.7 ± 4.8	87.6 ± 13.5	87.3 ± 2.1	75.4 ± 13.0	III
H230Y	Targeted	106.7 ± 9.7	102.3 ± 10.3	64.1 ± 3.5	39.4 ± 3.9	III
H230IHA	HA + linker	103.8 ± 7.3	75.8 ± 13	5.9 ± 2.2	5.3 ± 3.1	I
R250HA	HA insertion	72.3 ± 8.6	86.2 ± 4	10.2 ± 2.6	82.5 ± 7	II
D251A	Targeted	55.7 ± 3.9	50.9 ± 5.4	76.6 ± 3.9	83.2 ± 5.2	III
R248A-R250A	Charged	43.4 ± 12.3	128.9 ± 4.9	30.2 ± 8.5	68.5 ± 15.0	II
I252A	Hydrophobic	70.5 ± 7.5	50.5 ± 8.3	88.3 ± 1.6	91.8 ± 4.3	III
Y253N	N-gly addition	47.7 ± 8.3	84.9 ± 7.2	54.4 ± 15.0	47.2 ± 10.9	III

[a]I, transduction reduced in both cell types; II, transduction reduced in HAP1 cells compared to HAP1-ΔDAG cells; III, no receptor binding defects.

fusion assay because this pH produced the most syncytia (46, 47; data not shown). We speculate that LAMP1 may facilitate fusion pore formation at a more alkaline pH, thereby increasing the efficiency of LASV entry (30). The fusion assay may be able to circumvent the LAMP1 requirement with a more acidic environment, triggering fusion pore formation without LAMP1 interaction. This would explain why mutants can produce large syncytia when exogenous buffer is added yet are unable to productively enter cells on a pseudotyped particle. Removal of LAMP1 from cells dramatically decreases LASV entry efficiency but does not eliminate it (20). Perhaps some virions

encounter lysosomes with lower pH ranges, and the extra-acidic environment overcomes the LAMP1 requirement, similar to what is observed in the cell-to-cell fusion assay.

LASV entry requires interactions with both cell surface receptors and an internal receptor, LAMP1 (20). As previously mentioned, we identified a number of constructs that blocked entry into both cell types tested: H92A-H93A, 150lHA, 172HA, and 230lHA mutants. Both H92-H93 and H230 have been previously implicated in GP1-LAMP1 interaction (33). Protonation of the histidine residues may facilitate conformational changes that expose the LAMP1 binding site (30), which cryo-ET reconstructions suggest occurs in grooves between GP1 monomers that form under low-pH conditions (31). While histidines at positions 92, 93, and 230 may facilitate the low-pH conformational changes, 150lHA and 172HA fall on the opposite face of the crystal structure. If LAMP1 binding is occurring in a low-pH-induced groove, both 150lHA and 172HA may sterically prevent LAMP1 binding or cause premature shedding of GP1 from the glycoprotein complex. We did not identify any individual point mutations that prevented entry into both cell lines that were not previously associated with inducing low-pH conformational changes, suggesting that further work is required to locate the specific residues directly involved in LAMP1 interaction.

While most constructs efficiently entered both cell lines, those containing mutations between amino acids 141 and 150 and between amino acids 248 and 250 of GP1 demonstrated reduced transduction in HAP1 cells expressing αDG. A coimmunoprecipitation using VSV-pseudotyped particles confirmed the role of residues H141, F147, R248, and R250 in direct αDG binding. Residues H141, N146, F147, and Y150 face the 3-fold axis of the trimer, forming a putative receptor binding site (Fig. 9B, shown in red). A similar region within lymphocytic choriomeningitis virus (LCMV) has been implicated in LCMV GP1-αDG interaction (22). Previous biochemical studies show that the Old World (OW) arenavirus monomeric GP1 is unable to interact with αDG, which supports a binding site that requires an intact trimer (20, 22, 33). Residues R248 and R250 also face this center axis but are located deeper in the core (Fig. 9B, shown in orange). Presumably, αDG would not be interacting with the buried center of the trimer, but removal of the charged residues may alter the conformation of the domain above. K125A-K126A and 227HA modestly reduced HAP1 transduction and are located further away from the trimeric center. These mutations may exert long-range conformational changes that alter the αDG binding site (Fig. 9B, shown in yellow). For example, K125 and K126 line the GP1-GP1 interface within the trimer and therefore may play a role in maintaining the center conformation.

In 2015, the largest screen of LASV genomes revealed that isolates are highly heterogeneous and group by geographic distribution (48). The GP1 subunit had the highest sequence diversity of the four viral proteins, presumably due to continuous immune selection. When comparing the GP1 subunit among the 180 sequences collected, 68% of the amino acid sequence was conserved. However, the regions that we identified in this study that mediate αDG entry were 98 to 100% conserved, suggesting that these residues are important for the structure or function of GP1. The few residues that differed contained conservative amino acid substitutions. Several additional Old World arenaviruses, including LCMV, Mopeia virus (MOPV), and Mobala virus (MOBV), use αDG as their primary surface receptor (49). A GP1 sequence alignment of these four viruses reveals that the regions that we identified in LASV-αDG engagement are similar among these Old World arenaviruses (Fig. 9C). Furthermore, LCMV shares 63% sequence identity with LASV, and similar regions on GP1 have been implicated in LCMV's GP1-αDG binding site (22). Five residues that enhance LCMV GP1 binding to αDG have been identified: H136, S153, Y155, R190, and L260 (22, 50–54). Residues S153, Y155, R190, and L260 are located in the same region on GP1, which faces the 3-fold trimer axis (22), further supporting this region's importance in αDG binding.

In summary, our data suggest that the αDG binding site on LASV GP1 is found at the top central core of the GP trimer. These data correlate with the hypothesized αDG

binding regions within LCMV GP1 (22). Our data support the hypothesis that the histidine triad plays a role in the pH conformational changes required for LAMP1 interaction. In addition, we identify two HA insertion mutants, 150HA and 172HA, that may sterically block LAMP1 binding. Knowledge gained by this study will aid the development of small-molecule inhibitors to block LASV entry through its receptors αDG and LAMP1.

MATERIALS AND METHODS

Cell lines and transfections. Vero (African green monkey kidney) cells stably expressing human SLAM were maintained in Dulbecco's modified Eagle's medium (DMEM) supplemented with 5% (vol/vol) fetal bovine serum (FBS) at 37°C and 5% CO_2 (55). HAP1 and HAP1-ΔDAG1 cells (Horizon Discovery) were maintained in Iscove's medium supplemented with 10% (vol/vol) FBS at 37°C and 5% CO_2. All transient transfections were performed using GeneJuice (Millipore) as per the manufacturer's instruction.

Molecular biology. The LASV GPC protein coding sequence was codon optimized for mammalian expression and cloned into a pcDNA3.1intron vector. Gene expression was initiated by a cytomegalovirus (CMV) promoter, and the β-globin intron was engineered in the 5' untranslated region (UTR) to increase protein production. A carboxy-terminal 3× FLAG tag was added to the cytoplasmic tail of the GP2 subunit for biochemical detection. The HA tag coding sequence (YPYDVPDYA) was added to the plasmid at the indicated locations using PCR-based insertional mutagenesis with Q5 polymerase (NEB). Point mutations were introduced with QuikChange mutagenesis and PfuTurbo-HS polymerase (Agilent). The plasmid DNA of each construct was sequenced, and the presence of each mutation was confirmed. Complete sequence information is available upon request.

Surface biotinylation. Vero cells were transfected with plasmid DNA encoding the indicated Lassa virus GPC mutants. Thirty-six hours following transfection, cells were washed with cold PBS and biotinylated with 0.5 mg/ml sulfosuccinimidyl-2-(biotinamido) ethyl-1,3-dithiopropionate (Thermo) for 30 min on ice. The reaction was quenched using Tris-HCl, and cells were lysed in M2 lysis buffer (50 mM Tris [pH 7.4], 150 mM NaCl, 1 mM EDTA, 1% Triton X-100) at 4°C and clarified with centrifugation (20,000 × g, 15 min). Lysate was incubated with streptavidin Sepharose beads (GE Healthcare) for 60 min while rotating. Following incubation, the streptavidin Sepharose beads were washed in buffer 1 (100 mM Tris [40], 500 mM lithium chloride, 0.1% Triton X-100) and then in buffer 2 (20 mM HEPES [pH 7.2], 2 mM EGTA, 10 mM magnesium chloride, 0.1% Triton X-100), incubated in urea buffer (200 mM Tris [pH 6.8], 8 M urea, 5% sodium dodecyl sulfate [SDS], 0.1 mM EDTA, 0.03% bromophenol blue, 1.5% dithiothreitol [DTT]) for 30 min at 55°C, and subjected to immunoblot analysis.

Antibodies and immunoblots. Surface biotinylated material was fractionated by gel electrophoresis on 10% Tris-glycine gels (ThermoFisher) and transferred to polyvinylidene difluoride (PVDF) membranes (GE Healthcare). GP was detected with specific antibodies directed against the Flag epitope tag (M2; Sigma). Immunoblots were developed using mouse IgG horseradish peroxidase (HRP)-conjugated secondary antibodies (Jackson) and a ChemiDoc digital imaging system (Bio-Rad). Each experiment was repeated at least three independent times, and representative data or images are shown in the figures. Trichloroacetic acid (TCA)-precipitated pseudotyped particles were fractionated as described for biotinylated material. Protein was detected with specific antibodies directed against LASV GP2 (22.5D), kindly provided by James Robinson (Tulane University), and against VSV matrix (23H12; courtesy of Douglas Lyles; Kerafast) (56, 57). Alpha-dystroglycan was detected with IIH6 monoclonal antibody (EMD Millipore). Immunoblots were developed using HRP-conjugated human IgG and mouse IgG (Jackson) secondary antibodies, respectively, and a ChemiDoc digital imaging system (Bio-Rad). Immunoblot data were quantified using ImageLab software.

Cell-to-cell fusion assay. Vero cells were cotransfected with Lassa virus GP mutants and pmaxGFP (4:1 ratio). Forty hours following transfection, medium was removed and replaced with Dulbecco's PBS (DPBS) (pH 4) and incubated (37°C and 5% CO_2) for 30 min to allow glycoprotein triggering. The DPBS was replaced with DMEM, and cells were incubated for an additional 3 h to enable membrane rearrangement and clear syncytium formation. Four representative pictures of the fusion were taken using the Zoe microscope (Bio-Rad) (magnification, ×20), and unfused cells were counted. Quantification of fusion was calculated using the following equation: fusion = [(unfused cells in mock transfected − unfused cells in mutant transfected)/(unfused cells in mock transfected − unfused cells in WT GPC transfected)] × 100.

Each mutant was assessed in the fusion assay in three independent experiments.

VSV pseudotype production and transductions. GP constructs lacking the C-terminal 3× Flag tag were used to make the vesicular stomatitis virus (VSV)-pseudotyped particles. Vero cells were transfected with LASV GP DNA. Thirty-six hours following transfection, the cells were transduced with VSVΔG-GFP particles pseudotyped with VSV-G (multiplicity of infection [MOI], 1) for 1 h (courtesy of Michael Whitt; KeraFAST) (58). The particle-containing medium was then replaced with fresh DMEM. VSVΔG-GFP particles displaying the LASV GP were collected 12 h following the transduction. These particles were applied onto HAP1 and HAP1-ΔDAG1 cells in volumes of 0.25 ml and 1 ml, respectively. A higher volume of particles was used to transduce HAP1-ΔDAG1 cells in order to overcome the decreased transduction efficiency when the cells are missing the primary receptor (20). The number of GFP-positive cells was determined in a flow cytometer. Results are displayed as the percentage of GFP-positive cells present in a population of 10,000 live cell events compared to GP wild-type transduction. To monitor GP incorporation onto the VSV particles, 1 ml of precleared VSV transduction particles was precipitated using 10% (wt/vol) TCA. The TCA-treated proteins were pelleted (20,000 × g, 30 min, 4°C), washed with acetone,

dried, and denatured using SDS-urea buffer (200 mM Tris [pH 6.8], 8 M urea, 5% SDS, 0.1 mM EDTA, 0.03% bromophenol blue). Particles were subjected to immunoblot analysis for both VSV matrix levels and incorporated GP2.

Coimmunoprecipitation. Sheep polyclonal anti-human dystroglycan antibodies (R&D Systems) were bound to protein G beads (Bio-Rad) and incubated with αDG purified from rabbit muscle (59). The prepared beads were then divided equally into VSV-pseudotyped particles containing a normalized amount of GP and incubated for 1 h. Protein complexes were precipitated and washed three times with PBS. Bound proteins were eluted by incubating beads with urea-SDS plus DTT, heat denatured (56°C for 30 min), and separated on SDS-PAGE. Immunoblot analysis examined the amount of precipitated αDG and associated GP2.

REFERENCES

1. Frame JD, Baldwin JM, Jr, Gocke DJ, Troup JM. 1970. Lassa fever, a new virus disease of man from West Africa. I. Clinical description and pathological findings. Am J Trop Med Hyg 19:670–676.
2. Gunther S, Lenz O. 2004. Lassa virus. Crit Rev Clin Lab Sci 41:339–390. https://doi.org/10.1080/10408360490497456.
3. Mofolorunsho KC. 2016. Outbreak of lassa fever in Nigeria: measures for prevention and control. Pan Afr Med J 23:210. https://doi.org/10.11604/pamj.2016.23.210.8923.
4. Fichet-Calvet E, Rogers DJ. 2009. Risk maps of Lassa fever in West Africa. PLoS Negl Trop Dis 3:e388. https://doi.org/10.1371/journal.pntd.0000388.
5. Ogbu O, Ajuluchukwu E, Uneke CJ. 2007. Lassa fever in West African sub-region: an overview. J Vector Borne Dis 44:1–11.
6. Monath TP, Newhouse VF, Kemp GE, Setzer HW, Cacciapuoti A. 1974. Lassa virus isolation from Mastomys natalensis rodents during an epidemic in Sierra Leone. Science 185:263–265. https://doi.org/10.1126/science.185.4147.263.
7. Olayemi A, Cadar D, Magassouba N, Obadare A, Kourouma F, Oyeyiola A, Fasogbon S, Igbokwe J, Rieger T, Bockholt S, Jerome H, Schmidt-Chanasit J, Garigliany M, Lorenzen S, Igbahenah F, Fichet JN, Ortsega D, Omilabu S, Gunther S, Fichet-Calvet E. 2016. New hosts of the Lassa virus. Sci Rep 6:25280. https://doi.org/10.1038/srep25280.
8. Ajayi NA, Ukwaja KN, Ifebunandu NA, Nnabu R, Onwe FI, Asogun DA. 2014. Lassa fever—full recovery without ribavarin treatment: a case report. Afr Health Sci 14:1074–1077. https://doi.org/10.4314/ahs.v14i4.40.
9. Yun NE, Walker DH. 2012. Pathogenesis of Lassa fever. Viruses 4:2031–2048. https://doi.org/10.3390/v4102031.
10. Burri DJ, Pasqual G, Rochat C, Seidah NG, Pasquato A, Kunz S. 2012. Molecular characterization of the processing of arenavirus envelope glycoprotein precursors by subtilisin kexin isozyme-1/site-1 protease. J Virol 86:4935–4946. https://doi.org/10.1128/JVI.00024-12.
11. Kunz S, Edelmann KH, de la Torre JC, Gorney R, Oldstone MB. 2003. Mechanisms for lymphocytic choriomeningitis virus glycoprotein cleavage, transport, and incorporation into virions. Virology 314:168–178. https://doi.org/10.1016/S0042-6822(03)00421-5.
12. Beyer WR, Popplau D, Garten W, von Laer D, Lenz O. 2003. Endoproteolytic processing of the lymphocytic choriomeningitis virus glycoprotein by the subtilase SKI-1/S1P. J Virol 77:2866–2872. https://doi.org/10.1128/JVI.77.5.2866-2872.2003.
13. Lenz O, ter Meulen J, Klenk HD, Seidah NG, Garten W. 2001. The Lassa virus glycoprotein precursor GP-C is proteolytically processed by subtilase SKI-1/S1P. Proc Natl Acad Sci U S A 98:12701–12705. https://doi.org/10.1073/pnas.221447598.
14. Bederka LH, Bonhomme CJ, Ling EL, Buchmeier MJ. 2014. Arenavirus stable signal peptide is the keystone subunit for glycoprotein complex organization. mBio 5:e02063. https://doi.org/10.1128/mBio.02063-14.
15. Messina EL, York J, Nunberg JH. 2012. Dissection of the role of the stable signal peptide of the arenavirus envelope glycoprotein in membrane fusion. J Virol 86:6138–6145. https://doi.org/10.1128/JVI.07241-11.
16. Eichler R, Lenz O, Strecker T, Garten W. 2003. Signal peptide of Lassa virus glycoprotein GP-C exhibits an unusual length. FEBS Lett 538:203–206. https://doi.org/10.1016/S0014-5793(03)00160-1.
17. Briknarova K, Thomas CJ, York J, Nunberg JH. 2011. Structure of a zinc-binding domain in the Junin virus envelope glycoprotein. J Biol Chem 286:1528–1536. https://doi.org/10.1074/jbc.M110.166025.
18. York J, Nunberg JH. 2007. A novel zinc-binding domain is essential for formation of the functional Junin virus envelope glycoprotein complex. J Virol 81:13385–13391. https://doi.org/10.1128/JVI.01785-07.
19. York J, Nunberg JH. 2006. Role of the stable signal peptide of Junin arenavirus envelope glycoprotein in pH-dependent membrane fusion. J Virol 80:7775–7780. https://doi.org/10.1128/JVI.00642-06.
20. Jae LT, Raaben M, Herbert AS, Kuehne AI, Wirchnianski AS, Soh TK, Stubbs SH, Janssen H, Damme M, Saftig P, Whelan SP, Dye JM, Brummelkamp TR. 2014. Virus entry. Lassa virus entry requires a trigger-induced receptor switch. Science 344:1506–1510. https://doi.org/10.1126/science.1252480.
21. Cao W, Henry MD, Borrow P, Yamada H, Elder JH, Ravkov EV, Nichol ST, Compans RW, Campbell KP, Oldstone MB. 1998. Identification of alpha-dystroglycan as a receptor for lymphocytic choriomeningitis virus and Lassa fever virus. Science 282:2079–2081. https://doi.org/10.1126/science.282.5396.2079.
22. Hastie KM, Igonet S, Sullivan BM, Legrand P, Zandonatti MA, Robinson JE, Garry RF, Rey FA, Oldstone MB, Saphire EO. 2016. Crystal structure of the prefusion surface glycoprotein of the prototypic arenavirus LCMV. Nat Struct Mol Biol 23:513–521. https://doi.org/10.1038/nsmb.3210.
23. Igonet S, Vaney MC, Vonrhein C, Bricogne G, Stura EA, Hengartner H, Eschli B, Rey FA. 2011. X-ray structure of the arenavirus glycoprotein GP2 in its postfusion hairpin conformation. Proc Natl Acad Sci U S A 108:19967–19972. https://doi.org/10.1073/pnas.1108910108.
24. Eschli B, Quirin K, Wepf A, Weber J, Zinkernagel R, Hengartner H. 2006. Identification of an N-terminal trimeric coiled-coil core within arenavirus glycoprotein 2 permits assignment to class I viral fusion proteins. J Virol 80:5897–5907. https://doi.org/10.1128/JVI.00008-06.
25. Shimojima M, Stroher U, Ebihara H, Feldmann H, Kawaoka Y. 2012. Identification of cell surface molecules involved in dystroglycan-independent Lassa virus cell entry. J Virol 86:2067–2078. https://doi.org/10.1128/JVI.06451-11.
26. Goncalves AR, Moraz ML, Pasquato A, Helenius A, Lozach PY, Kunz S. 2013. Role of DC-SIGN in Lassa virus entry into human dendritic cells. J Virol 87:11504–11515. https://doi.org/10.1128/JVI.01893-13.
27. Rojek JM, Sanchez AB, Nguyen NT, de la Torre JC, Kunz S. 2008. Different mechanisms of cell entry by human-pathogenic Old World and New World arenaviruses. J Virol 82:7677–7687. https://doi.org/10.1128/JVI.00560-08.
28. Oppliger J, Torriani G, Herrador A, Kunz S. 2016. Lassa virus cell entry via dystroglycan involves an unusual pathway of macropinocytosis. J Virol https://doi.org/10.1128/JVI.00257-16.
29. Nunberg JH, York J. 2012. The curious case of arenavirus entry, and its inhibition. Viruses 4:83–101. https://doi.org/10.3390/v4010083.
30. Cohen-Dvashi H, Israeli H, Shani O, Katz A, Diskin R. 2016. Role of LAMP1 binding and pH sensing by the spike complex of Lassa virus. J Virol 90:10329–10338. https://doi.org/10.1128/JVI.01624-16.
31. Li S, Sun Z, Pryce R, Parsy ML, Fehling SK, Schlie K, Siebert CA, Garten W, Bowden TA, Strecker T, Huiskonen JT. 2016. Acidic pH-induced confor-

mations and LAMP1 binding of the Lassa virus glycoprotein spike. PLoS Pathog 12:e1005418. https://doi.org/10.1371/journal.ppat.1005418.

32. Hastie KM, Zandonatti MA, Kleinfelter LM, Heinrich ML, Rowland MM, Chandran K, Branco LM, Robinson JE, Garry RF, Saphire EO. 2017. Structural basis for antibody-mediated neutralization of Lassa virus. Science 356:923–928. https://doi.org/10.1126/science.aam7260.

33. Cohen-Dvashi H, Cohen N, Israeli H, Diskin R. 2015. Molecular mechanism for LAMP1 recognition by Lassa virus. J Virol 89:7584–7592. https://doi.org/10.1128/JVI.00651-15.

34. Bonhomme CJ, Capul AA, Lauron EJ, Bederka LH, Knopp KA, Buchmeier MJ. 2011. Glycosylation modulates arenavirus glycoprotein expression and function. Virology 409:223–233. https://doi.org/10.1016/j.virol.2010.10.011.

35. Eichler R, Lenz O, Garten W, Strecker T. 2006. The role of single N-glycans in proteolytic processing and cell surface transport of the Lassa virus glycoprotein GP-C. Virol J 3:41. https://doi.org/10.1186/1743-422X-3-41.

36. Jae LT, Raaben M, Riemersma M, van Beusekom E, Blomen VA, Velds A, Kerkhoven RM, Carette JE, Topaloglu H, Meinecke P, Wessels MW, Lefeber DJ, Whelan SP, van Bokhoven H, Brummelkamp TR. 2013. Deciphering the glycosylome of dystroglycanopathies using haploid screens for Lassa virus entry. Science 340:479–483. https://doi.org/10.1126/science.1233675.

37. Gallagher P, Henneberry J, Wilson I, Sambrook J, Gething MJ. 1988. Addition of carbohydrate side chains at novel sites on influenza virus hemagglutinin can modulate the folding, transport, and activity of the molecule. J Cell Biol 107:2059–2073. https://doi.org/10.1083/jcb.107.6.2059.

38. Tsuchiya E, Sugawara K, Hongo S, Matsuzaki Y, Muraki Y, Li ZN, Nakamura K. 2002. Effect of addition of new oligosaccharide chains to the globular head of influenza A/H2N2 virus haemagglutinin on the intracellular transport and biological activities of the molecule. J Gen Virol 83:1137–1146. https://doi.org/10.1099/0022-1317-83-5-1137.

39. Paal T, Brindley MA, St Clair C, Prussia A, Gaus D, Krumm SA, Snyder JP, Plemper RK. 2009. Probing the spatial organization of measles virus fusion complexes. J Virol 83:10480–10493. https://doi.org/10.1128/JVI.01195-09.

40. Radoshitzky SR, Longobardi LE, Kuhn JH, Retterer C, Dong L, Clester JC, Kota K, Carra J, Bavari S. 2011. Machupo virus glycoprotein determinants for human transferrin receptor 1 binding and cell entry. PLoS One 6:e21398. https://doi.org/10.1371/journal.pone.0021398.

41. Zavorotinskaya T, Albritton LM. 1999. A hydrophobic patch in ecotropic murine leukemia virus envelope protein is the putative binding site for a critical tyrosine residue on the cellular receptor. J Virol 73:10164–10172.

42. Apte-Sengupta S, Navaratnarajah CK, Cattaneo R. 2013. Hydrophobic and charged residues in the central segment of the measles virus hemagglutinin stalk mediate transmission of the fusion-triggering signal. J Virol 87:10401–10404. https://doi.org/10.1128/JVI.01547-13.

43. Bae Y, Kingsman SM, Kingsman AJ. 1997. Functional dissection of the Moloney murine leukemia virus envelope protein gp70. J Virol 71:2092–2099.

44. Wang WK, Dudek T, Essex M, Lee TH. 1999. Hypervariable region 3 residues of HIV type 1 gp120 involved in CCR5 coreceptor utilization: therapeutic and prophylactic implications. Proc Natl Acad Sci U S A 96:4558–4562. https://doi.org/10.1073/pnas.96.8.4558.

45. Johnson DE, Ostrowski P, Jaumouille V, Grinstein S. 2016. The position of lysosomes within the cell determines their luminal pH. J Cell Biol 212:677–692. https://doi.org/10.1083/jcb.201507112.

46. Cosset FL, Marianneau P, Verney G, Gallais F, Tordo N, Pecheur EI, ter Meulen J, Deubel V, Bartosch B. 2009. Characterization of Lassa virus cell entry and neutralization with Lassa virus pseudoparticles. J Virol 83:3228–3237. https://doi.org/10.1128/JVI.01711-08.

47. Klewitz C, Klenk HD, ter Meulen J. 2007. Amino acids from both N-terminal hydrophobic regions of the Lassa virus envelope glycoprotein GP-2 are critical for pH-dependent membrane fusion and infectivity. J Gen Virol 88:2320–2328. https://doi.org/10.1099/vir.0.82950-0.

48. Andersen KG, Shapiro BJ, Matranga CB, Sealfon R, Lin AE, Moses LM, Folarin OA, Goba A, Odia I, Ehiane PE, Momoh M, England EM, Winnicki S, Branco LM, Gire SK, Phelan E, Tariyal R, Tewhey R, Omoniwa O, Fullah M, Fonnie R, Fonnie M, Kanneh L, Jalloh S, Gbakie M, Saffa S, Karbo K, Gladden AD, Qu J, Stremlau M, Nekoui M, Finucane HK, Tabrizi S, Vitti JJ, Birren B, Fitzgerald M, McCowan C, Ireland A, Berlin AM, Bochicchio J, Tazon-Vega B, Lennon NJ, Ryan EM, Bjornson Z, Milner DA, Jr, Lukens AK, Broodie N, Rowland M, Heinrich M, Akdag M, Schieffelin JS, Levy D, Akpan H, Bausch DG, Rubins K, McCormick JB, Lander ES, Günther S, Hensley L, Okogbenin S, Viral Hemorrhagic Fever Consortium, Schaffner SF, Okokhere PO, Khan SH, Grant DS, Akpede GO, Asogun DA, Gnirke A, Levin JZ, Happi CT, Garry RF, Sabeti PC. 2015. Clinical sequencing uncovers origins and evolution of Lassa virus. Cell 162:738–750. https://doi.org/10.1016/j.cell.2015.07.020.

49. Kunz S. 2009. Receptor binding and cell entry of Old World arenaviruses reveal novel aspects of virus-host interaction. Virology 387:245–249. https://doi.org/10.1016/j.virol.2009.02.042.

50. Sullivan BM, Emonet SF, Welch MJ, Lee AM, Campbell KP, de la Torre JC, Oldstone MB. 2011. Point mutation in the glycoprotein of lymphocytic choriomeningitis virus is necessary for receptor binding, dendritic cell infection, and long-term persistence. Proc Natl Acad Sci U S A 108:2969–2974. https://doi.org/10.1073/pnas.1019304108.

51. Sevilla N, Kunz S, Holz A, Lewicki H, Homann D, Yamada H, Campbell KP, de La Torre JC, Oldstone MB. 2000. Immunosuppression and resultant viral persistence by specific viral targeting of dendritic cells. J Exp Med 192:1249–1260. https://doi.org/10.1084/jem.192.9.1249.

52. Kunz S, Sevilla N, Rojek JM, Oldstone MB. 2004. Use of alternative receptors different than alpha-dystroglycan by selected isolates of lymphocytic choriomeningitis virus. Virology 325:432–445. https://doi.org/10.1016/j.virol.2004.05.009.

53. Teng MN, Borrow P, Oldstone MB, de la Torre JC. 1996. A single amino acid change in the glycoprotein of lymphocytic choriomeningitis virus is associated with the ability to cause growth hormone deficiency syndrome. J Virol 70:8438–8443.

54. Smelt SC, Borrow P, Kunz S, Cao W, Tishon A, Lewicki H, Campbell KP, Oldstone MB. 2001. Differences in affinity of binding of lymphocytic choriomeningitis virus strains to the cellular receptor alpha-dystroglycan correlate with viral tropism and disease kinetics. J Virol 75:448–457. https://doi.org/10.1128/JVI.75.1.448-457.2001.

55. Ono N, Tatsuo H, Hidaka Y, Aoki T, Minagawa H, Yanagi Y. 2001. Measles viruses on throat swabs from measles patients use signaling lymphocytic activation molecule (CDw150) but not CD46 as a cellular receptor. J Virol 75:4399–4401. https://doi.org/10.1128/JVI.75.9.4399-4401.2001.

56. Robinson JE, Hastie KM, Cross RW, Yenni RE, Elliott DH, Rouelle JA, Kannadka CB, Smira AA, Garry CE, Bradley BT, Yu H, Shaffer JG, Boisen ML, Hartnett JN, Zandonatti MA, Rowland MM, Heinrich ML, Martinez-Sobrido L, Cheng B, de la Torre JC, Andersen KG, Goba A, Momoh M, Fullah M, Gbakie M, Kanneh L, Koroma VJ, Fonnie R, Jalloh SC, Kargbo B, Vandi MA, Gbetuwa M, Ikponmwosa O, Asogun DA, Okokhere PO, Follarin OA, Schieffelin JS, Pitts KR, Geisbert JB, Kulakoski PC, Wilson RB, Happi CT, Sabeti PC, Gevao SM, Khan SH, Grant DS, Geisbert TW, Saphire EO, Branco LM, Garry RF. 2016. Most neutralizing human monoclonal antibodies target novel epitopes requiring both Lassa virus glycoprotein subunits. Nat Commun 7:11544. https://doi.org/10.1038/ncomms11544.

57. Lefrancois L, Lyles DS. 1982. The interaction of antibody with the major surface glycoprotein of vesicular stomatitis virus. I. Analysis of neutralizing epitopes with monoclonal antibodies. Virology 121:157–167.

58. Whitt MA. 2010. Generation of VSV pseudotypes using recombinant DeltaG-VSV for studies on virus entry, identification of entry inhibitors, and immune responses to vaccines. J Virol Methods 169:365–374. https://doi.org/10.1016/j.jviromet.2010.08.006.

59. Imperiali M, Thoma C, Pavoni E, Brancaccio A, Callewaert N, Oxenius A. 2005. O Mannosylation of alpha-dystroglycan is essential for lymphocytic choriomeningitis virus receptor function. J Virol 79:14297–14308. https://doi.org/10.1128/JVI.79.22.14297-14308.2005.